



## Supporting Information

for *Adv. Sci.*, DOI: 10.1002/advs.201902561

Ultrasml BiOI Quantum Dots with Efficient Renal Clearance  
for Enhanced Radiotherapy of Cancer

*Xin Wang, Zhao Guo, Chenyang Zhang, Shuang Zhu, Lele Li,  
Zhanjun Gu,\* and Yuliang Zhao*

## Supporting Information

### **Ultrasml BiOI Quantum Dots with Efficient Renal Clearance for Enhanced Radiotherapy of Cancer**

*Xin Wang<sup>#</sup>, Zhao Guo<sup>#</sup>, Chenyang Zhang, Shuang Zhu, Lele Li, Zhanjun Gu\*, Yuliang Zhao*

Dr. X. Wang, Dr. Z. Guo, Dr. C. Zhang, S. Zhu, Prof. Z. Gu

CAS Key Laboratory for Biomedical Effects of Nanomaterials and Nanosafety, Institute of High Energy Physics, Chinese Academy of Sciences, Beijing, 100049, China

E-mail: zjgu@ihep.ac.cn

Dr. X. Wang, Dr. Z. Guo, Dr. C. Zhang, Prof. Z. Gu, Prof. Y. Zhao

College of Materials Science and Optoelectronic Technology, University of Chinese Academy of Sciences, Beijing 100049, China

Prof. L. Li, Prof. Y. Zhao

CAS Center for Excellence in Nanoscience, National Center for Nanoscience and Technology of China, Chinese Academy of Sciences, Beijing, 100190, China

<sup>#</sup>These authors contributed equally to this work.

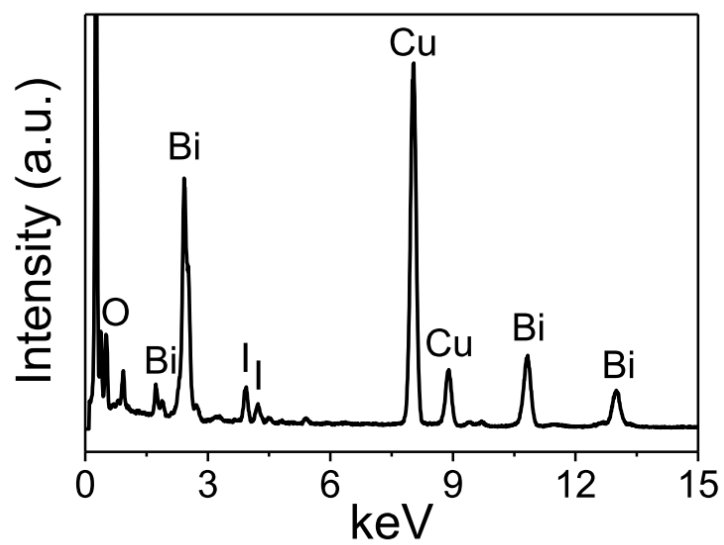


**Figure S1.** Energy-dispersive X-ray spectroscopy of BiOI QDs.

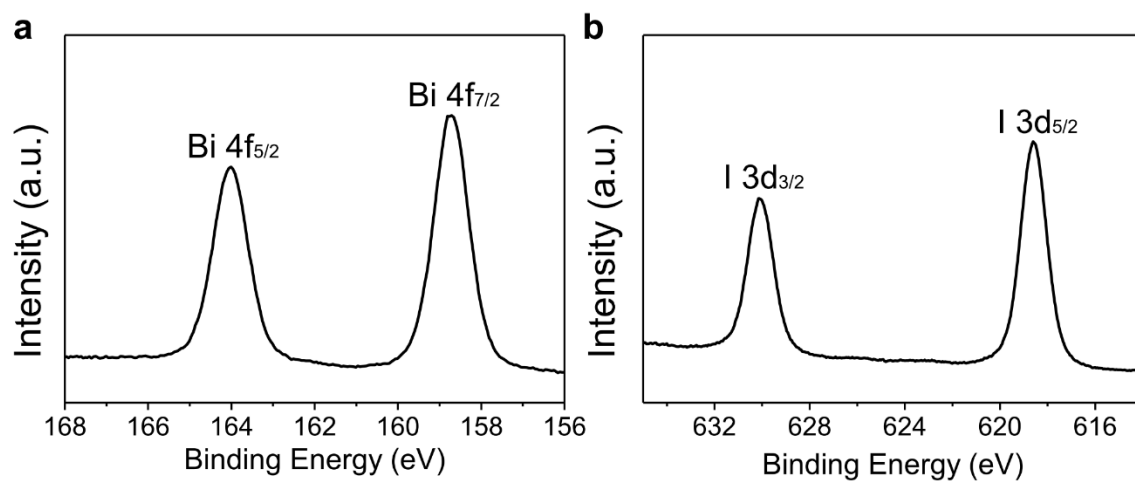


**Figure S2.** The high-resolution XPS spectra of (a) Bi 4f and (b) I 3d in BiOI QDs.

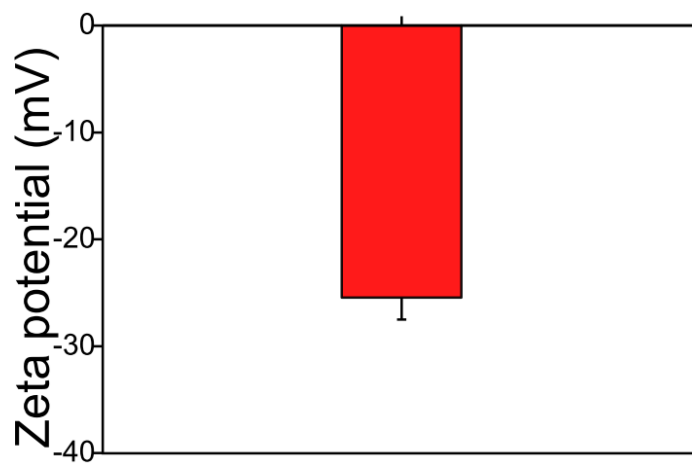


**Figure S3.** Zeta potential of as-prepared BiOI QDs.



H<sub>2</sub>O PBS RPMI FBS

**Figure S4.** Photograph of BiOI QDs dispersing in various physical solutions after 24 h.

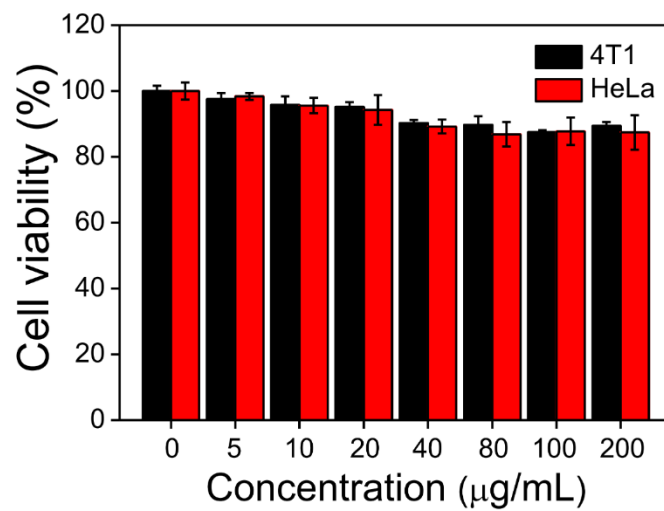


**Figure S5.** Cell viabilities of 4T1 cells and HeLa cells incubated with BiOI QDs of different concentrations for 24 h.

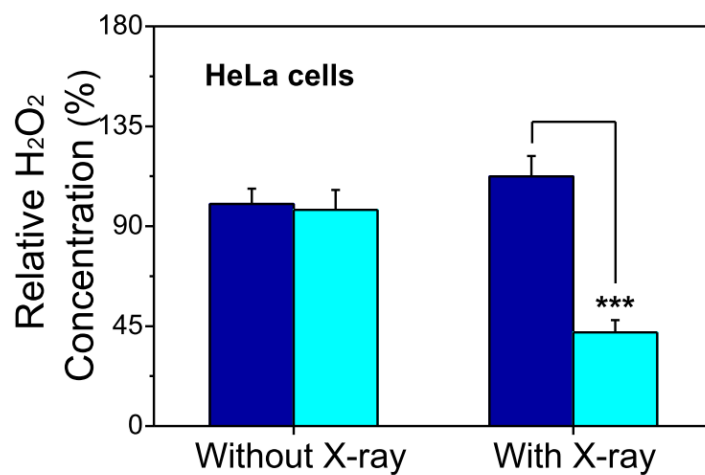


**Figure S6.** Detection of H<sub>2</sub>O<sub>2</sub> concentration in HeLa cells after various treatments. P values were calculated by the Student's t test: \*\*\*p < 0.001.



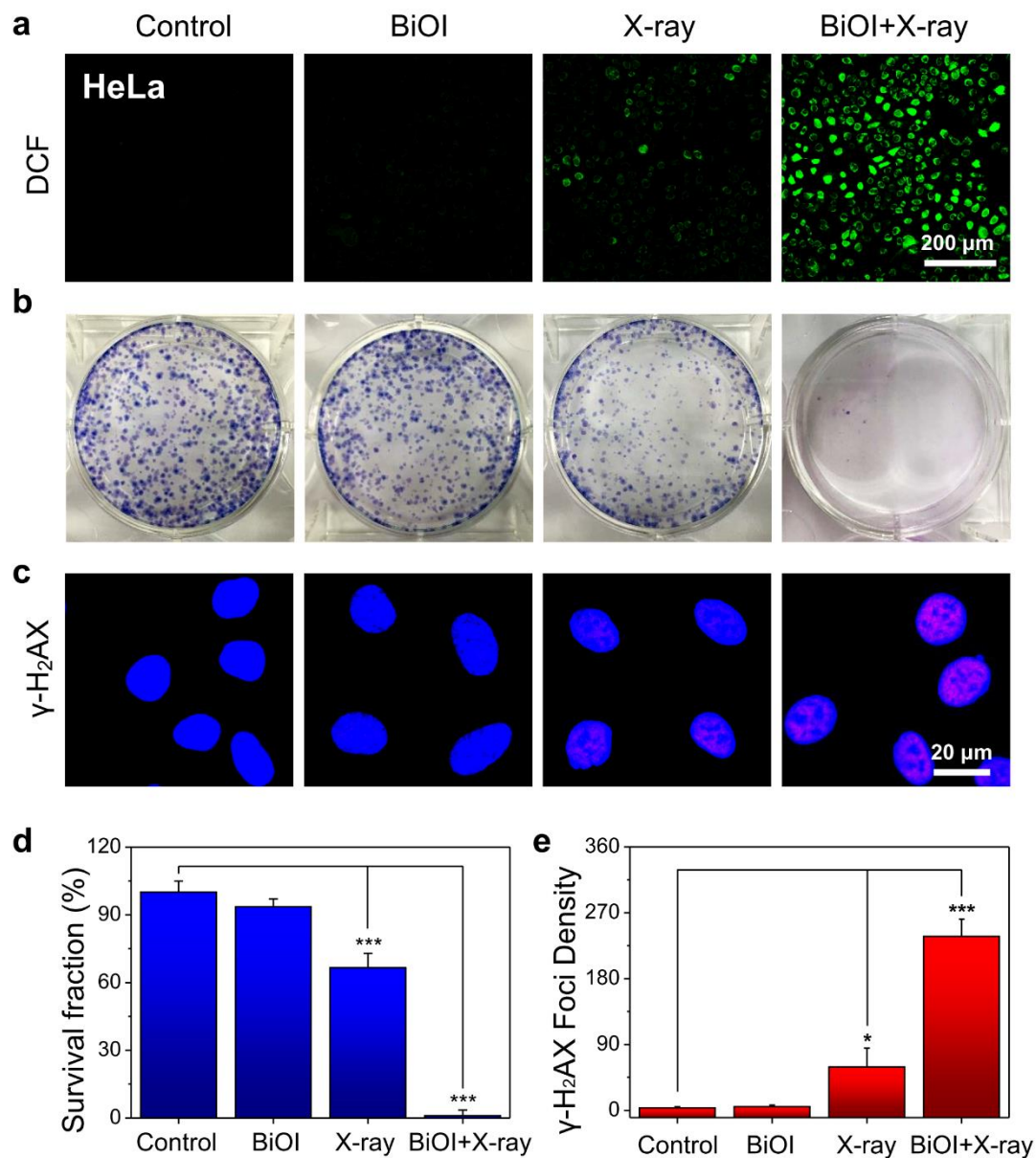


**Figure S7.** Enhanced radiotherapy of BiOI QDs in vitro on HeLa cells. a) ROS detection in HeLa cells. b) Colony formation after different treatments. c) Confocal images of DNA damage evaluated by  $\gamma\text{-H}_2\text{AX}$ . d) Survival fraction of each group from colony assay. e) Normalized  $\gamma\text{-H}_2\text{AX}$  fluorescence spot number after different treatments. P values were calculated by the Student's t test: \* $p < 0.05$ , \*\*\* $p < 0.001$ .

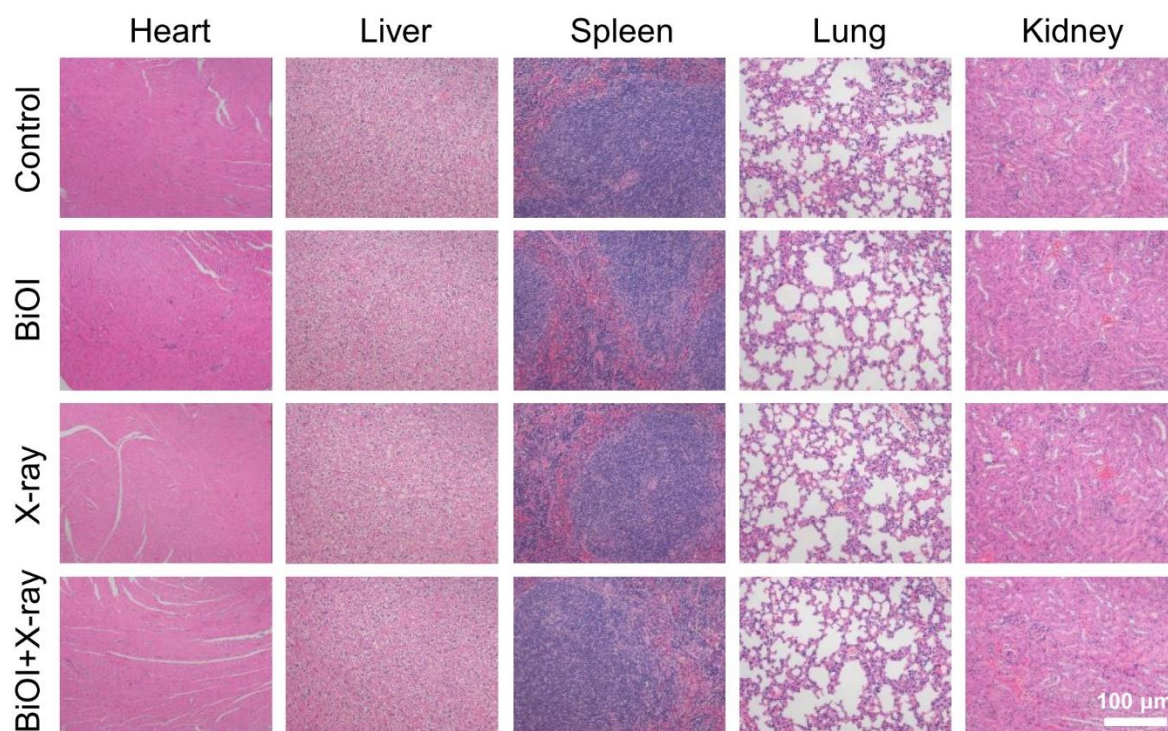


**Figure S8.** Representative H&E stained images of major organs from 4T1-tumor-bearing mice at the end of different treatments.

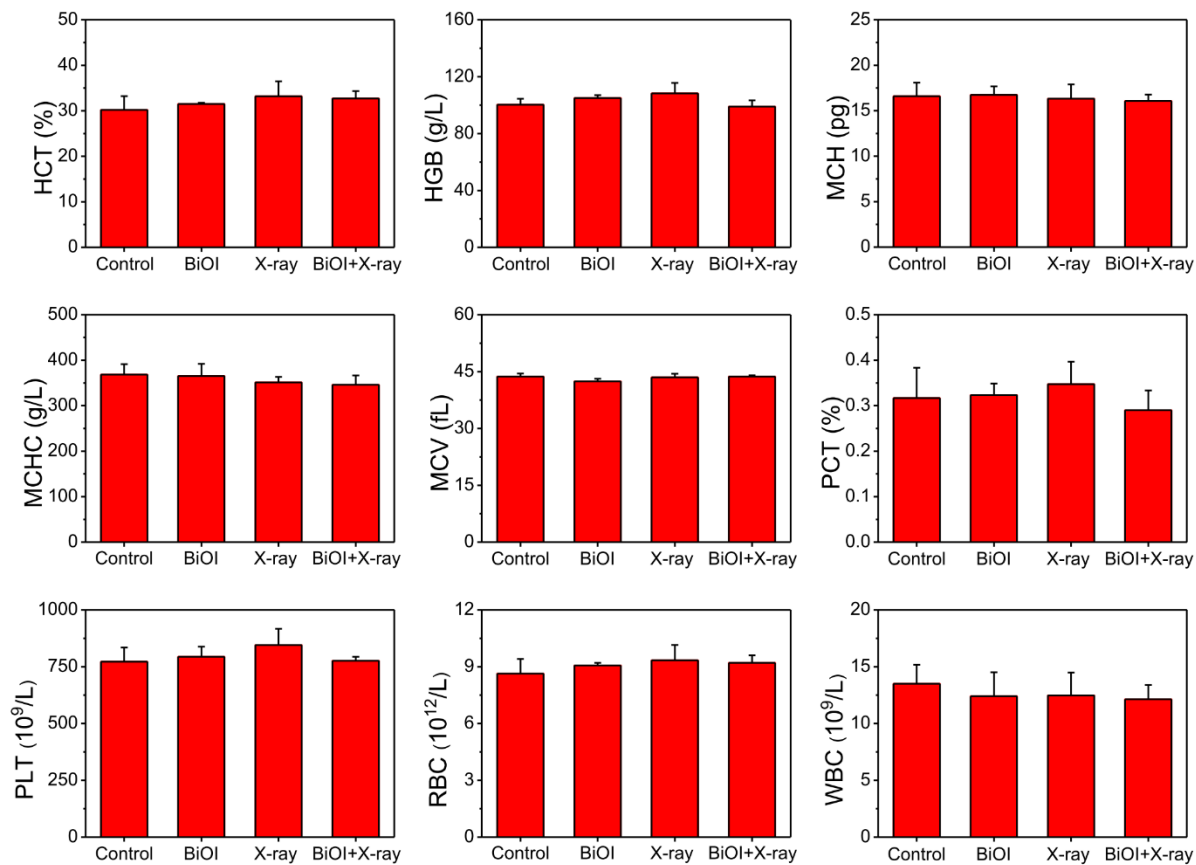


**Figure S9.** Blood hematology analyses of 4T1-tumor-bearing mice at the end of different treatments.

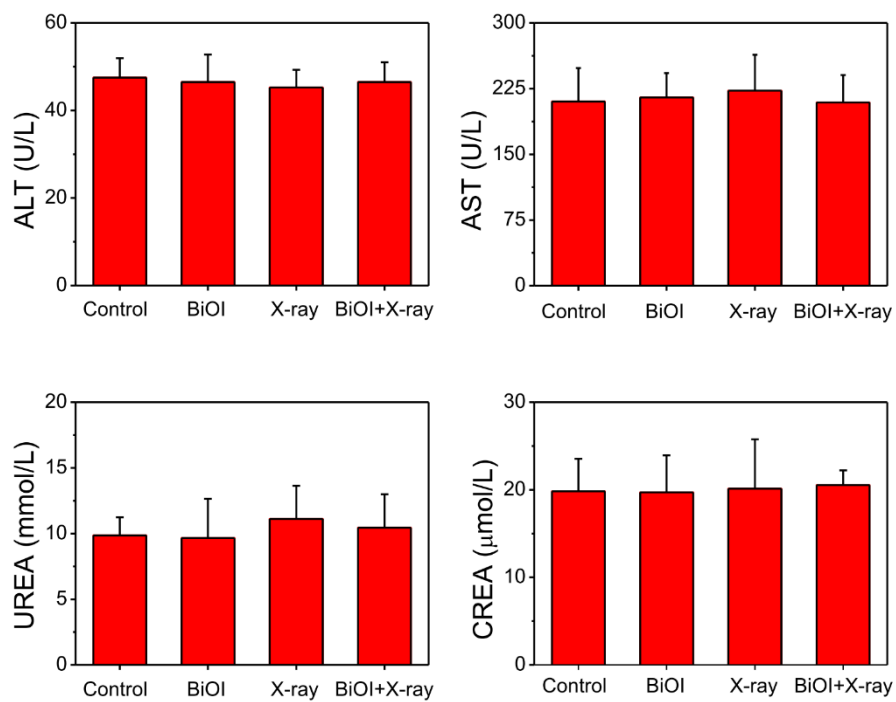


**Figure S10.** Blood biochemistry analyses of 4T1-tumor-bearing mice at the end of different treatments.

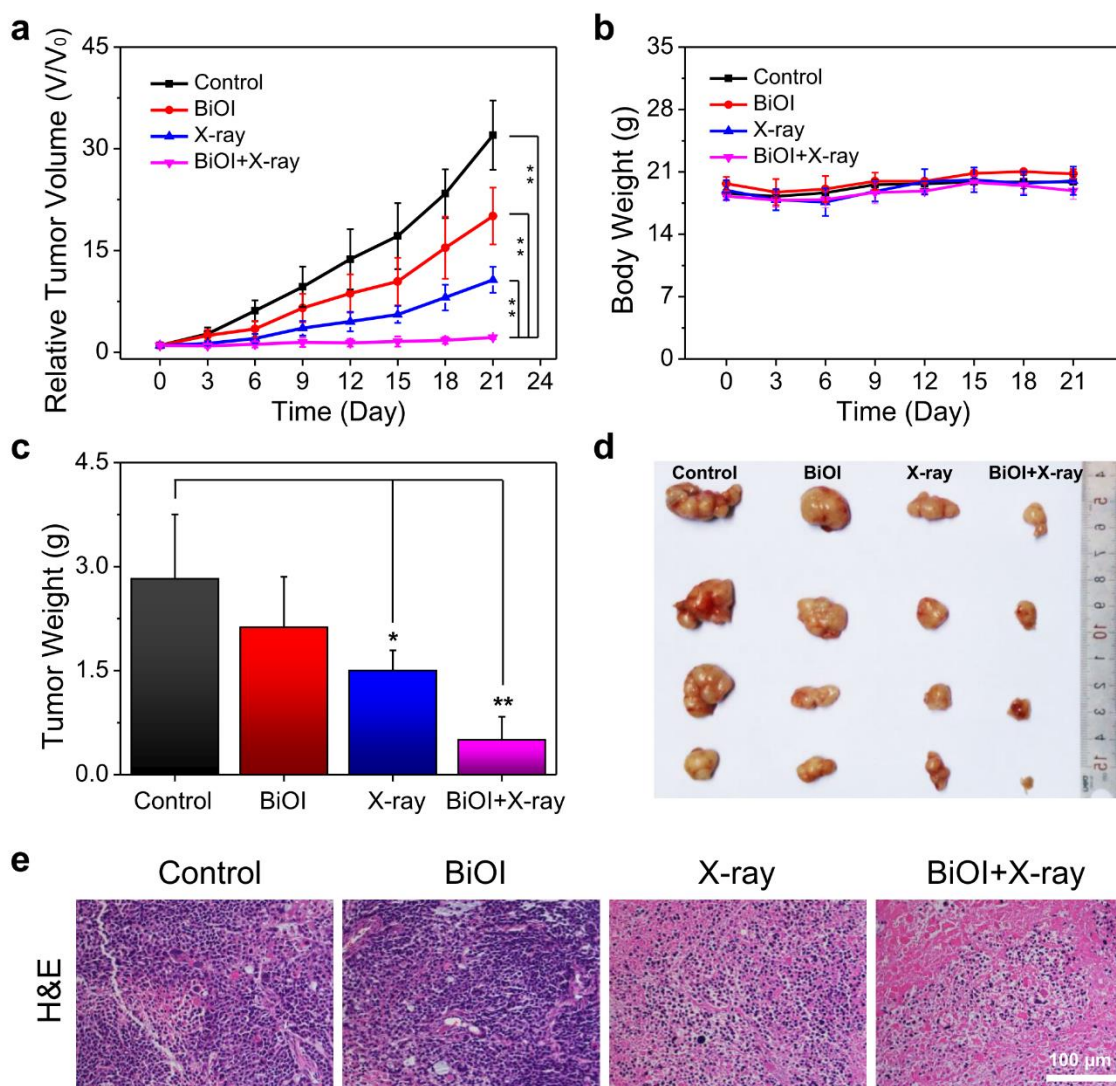


**Figure S11.** BiOI QDs sensitized radiotherapy in HeLa-tumor-bearing nude mice. a) Relative tumor volume profile of different groups: Control, BiOI, X-ray, BiOI + X-ray. b) Body weight of HeLa tumor bearing mice after treatments. c) Weights of excised tumors at 21st day after treatments. d) Photograph of excised tumors in each group at 21st day after treatments. e) Tumor images with H&E staining after treatments. P values were calculated by the Student's t test: \* $p < 0.05$ , \*\* $p < 0.01$ .

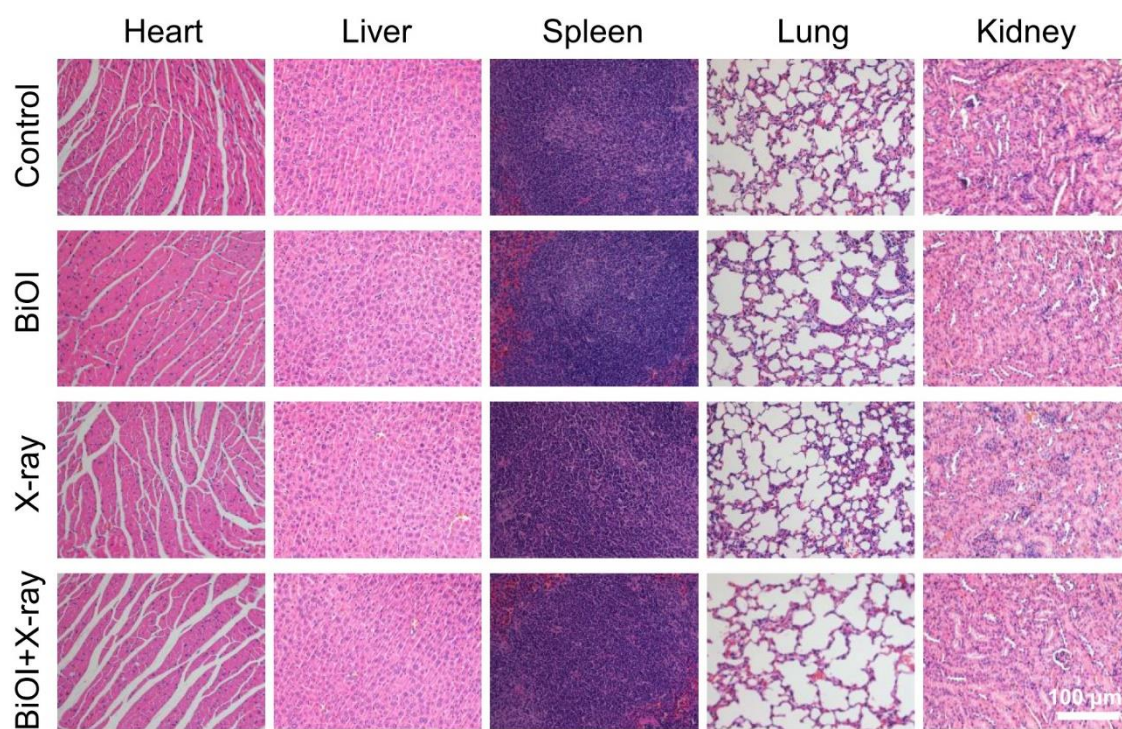


**Figure S12.** Representative H&E stained images of major organs from HeLa-tumor-bearing nude mice at the end of different treatments.

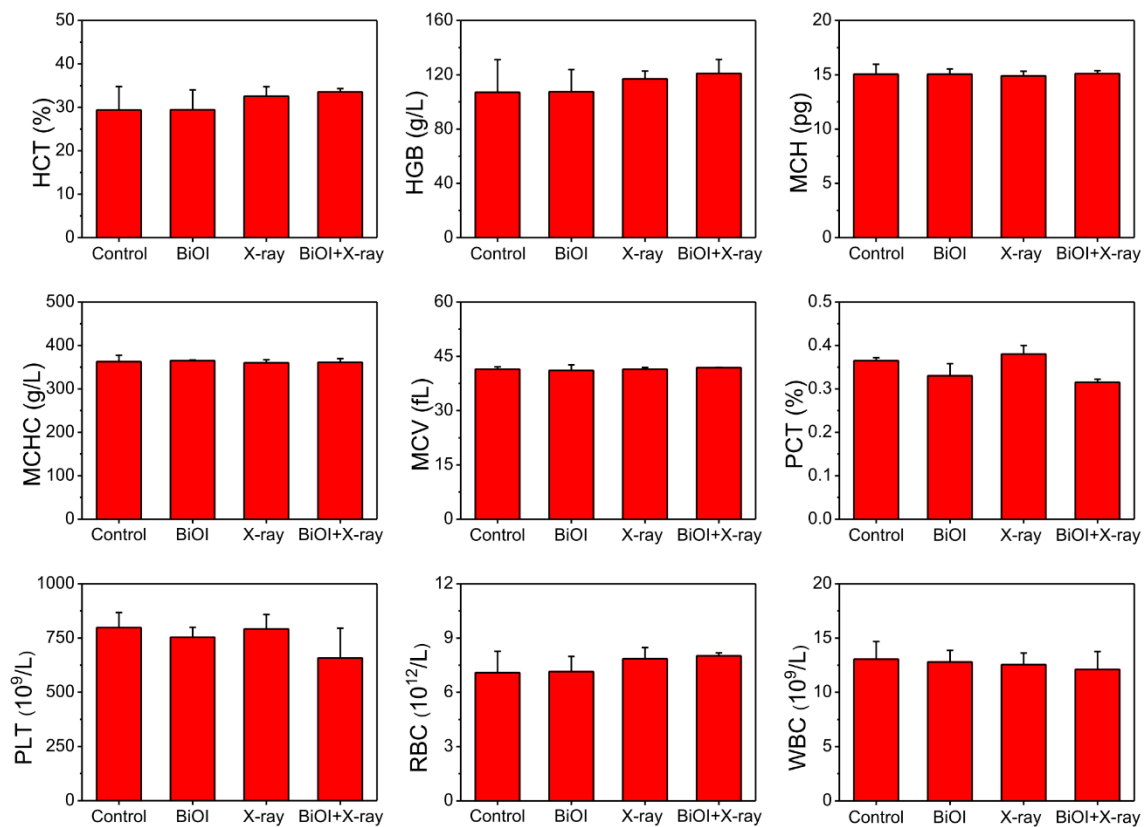


**Figure S13.** Blood hematology analyses of HeLa-tumor-bearing nude mice at the end of different treatments.

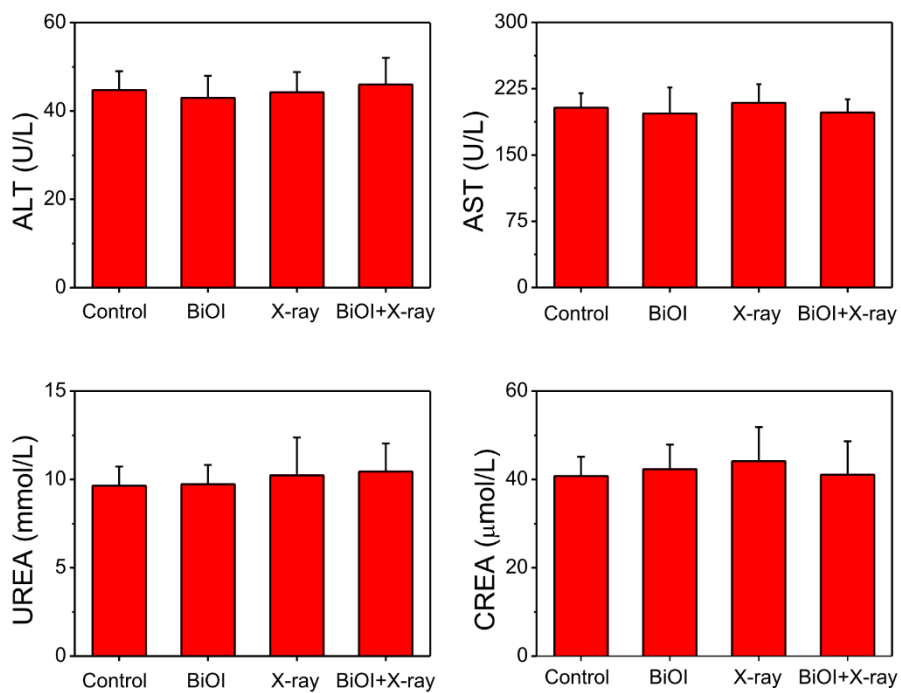


**Figure S14.** Blood biochemistry analyses of HeLa-tumor-bearing nude mice at the end of different treatments.